Retention of uranium in complexly altered of zircon: An example from Bancroft, Ontario*

Lutz Nasdala [a,†], **John M. Hanchar** [b], **Dieter Rhede** [c], **Allen K. Kennedy** [d], **Tamás Váczi** [a]

[a] *Institut für Mineralogie und Kristallographie, Universität Wien, A–1090 Wien, Austria*

[b] *Department of Earth Sciences, Memorial University of Newfoundland, St. John's, NL A1B 3X5, Canada*

[c] *Sektion 4.2, Anorganische und Isotopengeochemie, Helmholtz-Zentrum Potsdam, Deutsches GeoForschungsZentrum GFZ, D–14473 Potsdam, Germany*

[d] *Department of Imaging and Applied Physics, Curtin University of Technology, Perth, WA 6102, Australia*

* This paper is dedicated to Dr. Thomas E. Krogh (1936–2008), who made several outstanding contributions throughout his career to the radiometric dating of zircon, in particular through the development of new analytical techniques. Thomas Krogh had collected the sample that was studied in this contribution.

† Corresponding author.

E-mail address: lutz.nasdala@univie.ac.at (L. Nasdala).

A B S T R A C T

Mesoproterozoic (~1050 Ma; Stenian) zircon crystals from the Saranac Prospect, Bancroft, Ontario, contain up to ~1 wt% of U and ~0.15 wt% Th and, correspondingly, they are for the most part extensively radiation-damaged (calculated total α-doses 2.3–35.3 × 10^{18}/g). The crystals show textures of complex, intense chemical alteration that is attributed to multiple, low-*T* replacement events along fluid-controlled reaction fronts. Centers of crystals appear totally replaced; the primary zoning is virtually erased and the material has high porosity and numerous inclusions. Interior regions surrounding the central re-worked areas still exhibit primary igneous-type zoning; in those regions the alteration emanates from fractures and then follows the more radiation-damaged growth zones. Altered areas are typically recognized by their high porosity, low BSE intensity, and deficient analytical totals. Those regions often have lost a significant fraction of their radiogenic Pb. They are in general somewhat depleted in Zr, Si, and U, and are notably enriched in Ca and Fe. Element maps reveal elevated concentrations of Al and Y within filled fractures. Our observations indicate that the fluid-driven ion exchange is mainly controlled by the accessibility of micro-areas with elevated levels of radiation damage to transporting fluids via “fast pathways”. Most importantly, there is apparent Zr–Si–U equilibrium between initially existing and newly formed zircon. The retention of U after the chemical replacement (94±14 % relative to the original U content in the respective zones) does not significantly fall below the retention of two major cations Zr (95±4 %) and Si (95±2 %). In spite of the partially extreme hydrothermal alteration overprinting, the original U zoning in the crystals is well preserved. These observations suggest that preferential chemical leaching of U from zircon is clearly not a general feature of this mineral. This in turn seems to question the general validity of hydrothermal experiments to low-T, fluid-driven alteration of zircon in geological environments. The observed apparent immobility of U may affect the interpretation of U–Pb discordance in zircon, and the performance assessment of this mineral as potential waste form for actinides.

1. Introduction

Zircon ($ZrSiO_4$; $I4_1/amd$) is a common accessory phase in many rocks. This mineral is remarkably resistant against dissolution or chemical alteration over a wide range of geological environments and *P–T* conditions. Zircon normally incorporates, apart from Hf, low levels of non-formula elements. In particular, Pb is typically excluded in primary growth (Krogh, 1993) whereas radiogenic Pb, produced and "implanted" by radioactive decay of trace amounts of U and Th, is retained over billions of years as a result of the extremely low volume diffusion rate of Pb in zircon (Cherniak and Watson, 2001; 2003). Because of these extraordinary properties, zircon has been historically the mineral of choice for U–Th–Pb geochronology (e.g., Davis et al., 2003; and references therein).

The intrinsic physical properties and the chemical resistance of zircon, however, are dramatically affected by the accumulation of structural radiation damage, which is primarily produced by heavy recoil nuclei, and to a much lesser extent by the alpha particles ejected during the decay process, in alpha-decay events (Ewing, 1994; Weber et al., 1994; 1998; Nasdala et al., 2001). In the past two decades, zircon has also been proposed as a potential repository mineral for the long-term disposal of spent nuclear fuel and dismantled nuclear weapons (Ewing, 1999; 2001; Lumpkin, 2006). The performance assessment of zircon, and other U- and Th-bearing accessory minerals, as future host ceramic material for the long-term storage and isolation of heavy radionuclides therefore requires knowledge of irradiation effects, the accompanying changes of physical properties, and the response of variably radiation-damaged solids to changes of *P* and *T*. Research addressing these, and related questions, can be subdivided into three major groups: (i) studies of radiation effects and alteration processes in well-characterized natural samples, including their behavior in annealing and hydrothermal experiments; (ii) analogous studies of synthetic ceramic compounds doped with short-lived alpha emitters (e.g., ^{238}Pu, ^{237}Np, etc.), or samples that were irradiation-damaged through ion implantation in the laboratory; and (iii) theoretical *ab initio* studies and predictions such as molecular dynamics calculations (e.g., Ewing, 2001, Ewing et al., 2003).

The present study belongs to the first group. Thorough evaluation of natural alteration processes and their resulting effects adds to the knowledge on the chemical and physical stability of variably radiation-damaged accessory minerals in a low-*T* hydrothermal environment over extended geologic periods of time. It is well known that the behavior of zircon under such conditions may vary appreciably. First, this is controlled to a large extent by the amount of accumulated radiation damage, which in turn is directly related to the initial U and Th contents, and the respective distribution of those elements within the zircon structure. However, even though the dissolution kinetics of zircon [Lutz I still do not like the term “chemical leaching property” because it does not explain the process. Here is a suggestion] is enhanced as radiation damage accumulates in the crystal structure, radiation damage itself does not cause elemental losses but merely increases their probability (Davis and Krogh, 2000). The second major control of the chemical and physical stability of zircon is the thermal and potentially the chemical and physical alteration history; in the latter case especially the geochemical environment in which the zircon resided. Even the treatment of zircon with high purity water may result in notable loss of both Pb and U (Hansen and Friderichsen, 1989). In contrast, secondary Pb loss was insignificant in zircon that spent geologic periods immersed in connate water at moderately elevated *T* (Gentry et al. 1982); conditions expected in a nuclear repository. Caruba et al. (1974) summarized that zircon has a wide stability in acidic solutions whereas the chemical stability is notably lowered in alkaline environments. Also, hydrothermal experiments yielded variable results. Pidgeon et al. (1966) and Shukolyukov et al. (1994) observed that hydrothermal treatment of zircon resulted in notable Pb loss but insignificant U loss. Sinha et al. (1992) obtained similar results (e.g., strong Pb loss and moderate U loss); however, only upon hydrothermal treatment of zircon with 2% HNO_3 solution whereas Pb and U were almost equally depleted after treatment in a 2M NaCl solution. Preferential U loss from zircon was also reported by Prasad and Naidu (1971), Tole (1985), Mattinson (1994; 2005), and Geisler et al. (2002; 2003b). Rizvanova et al. (2000) observed that U gain and large Pb losses (connected with zircon decomposition) resulted from experiments in which the zircon crystals were subjected to a 1M NaOH solution. In contrast, treatment in 1M NaCl solution was found to result in Pb and especially U loss by these authors. These diverse results may suggest that in undertaking such hydrothermal experiments, more

care should be taken to select experimental conditions (especially the compositions of the fluids doing the alteration) that are relevant to natural environments. In the present study, we report results in the changes of the elemental and U–Pb isotopic compositions of a natural, highly radiation-damaged zircon sample that has undergone extreme chemical and physical alteration.

2. Materials and methods

The zircon sample investigated in this study, consisting of six large single-crystals zircons, were obtained from the late Dr. Thomas E. Krogh in 1997. The crystals came from the Saranac Prospect (also referred to as Saranac Property in some reports; see Satterly, 1957), Bancroft District, Ontario, Canada. They originate from a thorite-zircon-rich albite leucogranite, a granite pegmatite, or associated skarn rocks enriched in zircon and thorite (Satterly, 1957).

Microprobe mounts were produced by cutting crystals along the crystallographic *c*-axis, embedding them (together with ion microprobe calibration standards) in araldite epoxy, and then ground and polished to their crystal centers, to reveal internal textures of the crystals. For optical microscopy, doubly-polished thin sections attached to a glass slide, with thicknesses of ~30 μm, were prepared. Prior to electron microprobe and ion microprobe analysis, sample mounts were coated with carbon or gold, respectively.

Internal textures were inspected under an optical microscope, in plane-polarized and cross-polarized transmitted light. This technique was also used to determine the birefringence, whose decrease is a reliable estimate of the accumulated radiation damage (Morgan and Auer, 1941; Sahama, 1981; Chakoumakos et al., 1987). The degree of structural damage was also estimated from the broadening of the $\nu_3(SiO_4)$ Raman band (Nasdala et al., 1995). Raman spectra were obtained by means of a confocal Horiba Jobin Yvon LabRam HR800 spectrometer with 632.8 nm He-Ne excitation. More experimental details are reported elsewhere (Nasdala et al., 2005). Band fitting and determination of the full width at half-maximum (FWHM) was done

assuming Lorentzian-Gaussian band shapes. The mathematical correction of FWHMs for the experimental broadening (i.e., apparatus function) has been discussed in detail by Nasdala et al. (2001).

Back-scattered electron (BSE) images, and wavelength-dispersive X-ray analyses of the chemical composition, including element distribution maps, were obtained with a JEOL JXA-8500F electron probe micro-analyzer (EPMA) equipped with a thermal field emission electron gun. For individual spot analyses, the accelerating voltage was set to 15 kV and the beam current used was 20 nA. The electron beam was focused to a <0.1 μm spot. Calibration standards used were well-characterised natural and synthetic materials including zircon (Si, Zr), corundum (Al), hematite (Fe), vanadinite (Pb), phosphates (P, Y, Yb), HfO_2 (Hf), and metals (U, Th). The CITZAF routine in the JEOL software, which is based on the Φ(ρZ) method (Armstrong, 1995), was used for data processing. Element distribution maps, consisting of 250 × 200 pixels with inter-distances of 0.2–0.5 μm, were obtained with an accelerating voltage of 6–15 kV, a beam current of 10–40 nA, and a dwell time of 1–1.5 s per pixel. For more details see Keller et al. (2008).

Analyses of the U–Th–Pb isotopic composition were done using a SHRIMP II at Curtin University of Technology, Perth. The zircon surface was sputtered with a primary, mass-filtered $(O_2)^-$ beam with ~1 nA current, focused to a ~10 μm spot. The mass resolution, M/ΔM, was better than 5000. For more experimental details see DeLaeter and Kennedy (1998). To avoid mixed results due to the ion beam having straddled both unaltered and altered volumes, analysis spots were located carefully within the different regions, and only regions that appeared either fully unaltered or completely altered on a scale of at least 20–30 μm were analyzed in the SHRIMP. Results were calibrated against M257, a 561.3 Ma old reference zircon (Nasdala et al., 2008). Common Pb was assumed to have a Broken Hill Pb composition and was corrected for using the ^{204}Pb method (Compston et al., 1984). Data reduction was done using the ^{238}U decay constant of Jaffey et al. (1971; 1.55125×10^{-10}) and the revised ^{235}U decay constant of Schoene et al. (2006; 9.8569×10^{-10}). The Excel-based program Squid (Ludwig 2002) was used for data processing. Data were plotted using the Isoplot program (Ludwig 2003).

3. Results and discussion

3.1. Textural patterns of secondary alteration

Transmitted light photomicrographs of typical zircon crystals from the Saranac Prospect are shown in Figures 1 and 2a and b, and representative BSE images are presented in Figures 2c–f and 3. The zircon crystals range in size from several mm to approximately one cm, are dark brown in color, and have well-formed, euhedral prismatic shapes. In some of the grains, large inclusions of K-feldspar and/or α-quartz are present (e.g., left crystal in Fig. 1a).

The zircon crystals show complex internal textures, consisting of two main textural varieties (Fig. 1). First, a large majority of the interiors of the zircon crystals show growth zoning (often referred to as oscillatory zoning) that is characteristic of primary zircon growth in an igneous (Connelly, 2000; Hoskin, 2000; Corfu et al., 2003) or metasomatic environments (Smith et al., 1991). Second, there are extended regions, mostly close to the centers of crystals, in which the primary zoning for the most part has been obliterated. These regions show rather chaotic textural patterns and are rich in inclusions and both sub-micrometer sized and macroscopic pore spaces; the latter up to a few ten μm in size (Fig. 3). We will refer to the two textural types as “zoned” and “macro porous”. Zoned and macro-porous zircon regions were observed, though with moderate variations of their volume fractions (estimated ranges are 30–70 vol% each), in all six crystals studied.

The zoned regions in the zircon crystals are highly fractured, with a radial pattern (Fig. 2a–c) that we assign to differential volume expansion of neighboring zones with differing degrees of radiation damage (Peterman et al., 1986; Chakoumakos et al., 1987; Lee and Tromp, 1995; Nasdala et al., 1999; Sláma et al., 2008). There is no indication of hydraulic fracturing in these zircon crystals (cf. Rimša et al., 2007).

The zoned zircon is extensively altered, indicated by a significant volume fraction of areas with notably lower BSE intensities (Figs. 2c–f). The boundary of the altered patches to their neighboring high-BSE areas is

always sharp, reflecting a two-dimensional, fluid-driven alteration reaction front (cf. Geisler et al., 2003b; Labotka et al., 2004; Putnis et al., 2007; Pöml et al., 2007). In contrast, a gradual or transitional change in the BSE intensity would indicate a diffusional alteration reaction process; this is not observed. The altered, low-BSE micro-areas are located along fractures (Figs. 2c–e) or along the growth zoning (Figs. 2c, e, f).

The macro-porous zircon is characterized predominantly by very low BSE intensities (Fig. 3). Both the very low BSE intensities along with extensive porosity (e.g., Nasdala et al., 2009), and the apparent obliteration of the primary growth zoning, suggest that the macro-porous zircon has experienced extreme alteration, most probably through a fluid-driven replacement reaction process. The altered nature of the macro-porous zircon is indicated as well by the presence of numerous inclusions of phases that are typically not present in primary zircon (cf. Corfu, 2003; Johan and Johan, 2005; Breiter et al., 2006). The macro-porous zircon is especially rich in inclusions of high-BSE phases such as uranium oxide, uranium and thorium silicates, lead sulfide, and an unidentified yttrium silicate phase. Less abundant low-BSE inclusions include SiO_2, K-feldspar, and rarely apatite.

There is often a sharp, well-defined boundary between the two textural types (Fig. 1b), however, in some cases a gradual transition may also be observed. The sharp boundary follows in some cases the growth zoning whereas in other cases it does not. These observations seem to exclude that the zoned zircon overgrew the macro-porous zircon; rather the two textural types seem to represent different alteration products of the same primary zircon material.

3.2. Chemical changes during alteration

Electron microprobe analyses of the chemical composition of the zircon crystals studied are presented in Table 1. Analytical results vary appreciably, with a conspicuous correlation between the BSE intensity and the EPMA results.

Within the zoned zircon, most low-BSE areas have deficient analytical totals in the 94–98 wt% oxide range. These areas are notably depleted in SiO_2 and ZrO_2 whereas there are elevated levels of non-formula chemical elements including CaO (up to 3.1 wt%), FeO (up to 0.7 wt%), and in some cases Al_2O_3. High-BSE areas, in contrast, yielded rather "regular" stoichiometric SiO_2 and ZrO_2 values, almost no Ca, Fe, and Al, and much less deficient analytical totals (typically, 98–100 wt%). The non-formula constituents HfO_2, UO_2, and Y_2O_3 were detected in all areas, and they do not show any direct correlation with the BSE intensity. The strong variations of these elements among the eleven growth zones (labeled A–K in Table 1), however, suggest primary compositional zoning. All other non-formula elements were mostly close to, or below, the detection limit.

Similar results were obtained from the macro-porous zircon, though with a weaker correlation with the BSE intensity. The depletions in SiO_2 and ZrO_2 correlate with deficiencies in analytical totals and the BSE intensity. Higher-BSE regions have analytical totals between 97–98 wt%, and low-BSE regions between 92–97 wt%, (Table 1). Similar to the zoned zircon, CaO (1.7–3.8 wt%) and FeO (0.4–0.8 wt%) are clearly enriched in low-BSE areas of the macro-porous zircon but mostly not detected in high-BSE areas. As noted above, all other non-formula elements do not correlate with the BSE intensity.

Note that deficient analysis sums do not necessarily suggest the presence of a hydrous phase; even though the analytical shortfall of zircon EPMA analyses was sometimes assigned to a hypothetical "H_2O*" (e.g., Johan and Johan, 2005; Utsunomiya et al., 2007). Deficient totals, obtained for non-hydrous, porous solids (Lakis et al., 1992; Sorbier et al., 2004), are explained by charge trapping, pore geometry variation, and losses of X-ray quanta at interfaces. In the case of hydrothermally altered zircon, porosity (Figs. 2f and 3) is especially common because of radiation-damaged and hence volume-expanded zircon being replaced by crystalline zircon (Nasdala et al., 2009). Deficient totals, and the accompanying effect of very low BSE intensities in such areas (Figs. 2 and 3; cf. Pointer et al., 1988; Smith et al., 1991; Nasdala et al., 2009) are, therefore, strong indicators of secondary alteration.

Non-formula elements such as Ca, Al, and Fe (in contrast to Hf and the actinides U and Th) are normally excluded during primary zircon growth whereas they are typically observed in chemically altered zircon (Törnroos, 1985; Smith et al., 1991; Geisler et al., 2003a; Pérez-Soba et al., 2007). Those results are confirmed by EPMA analyses, which yielded elevated Ca and Fe concentrations only in the altered, low-BSE micro-areas adjacent to the primary zoned zircon regions. Phosphorous, however, which is also a common constituent in altered zircon (e.g., Mathieu et al., 2001; Tomaschek et al., 2003; Utsunomiya et al., 2007; Van Lichtervelde et al., 2009), was not detected in any of the six Saranac Prospect zircon crystals that were investigated. The results of this present study are similar to those of Krogh and Davis (1973; 1975) who found altered zircon to be depleted in Zr and Si, and enriched in Ca, Fe, and Al.

To study elemental changes upon alteration in more detail, high-resolution EPMA X-ray element mapping was done (Fig. 4). Distribution patterns vary appreciably between elements; they can be assigned to three principal groups: (i) Concentrations (or, more exactly, detected EPMA count rates) of Zr (Figs. 4a, b), Si (not shown), Hf (not shown), and U (Figs. 4a, b) are mainly determined by the strong primary chemical zoning. Alteration patterns (i.e., the comparably smaller concentration variations internal to unaltered and altered micro-areas) are recognized if only the upper portions of the count rate scales are used to generate color-coded distribution maps of these elements (e.g., Zr concentration distributions in Figs. 4a and b; compare count rate ranges given in the caption). The primary zoning is, though on a very low level and hence more noisy, also seen in the Y patterns (Fig. 4a); (ii) The distribution patterns of Ca (Figs. 4b, c) and Fe (not shown) are consistent with the BSE intensities and hence the locations of the alteration. These two elements always yield high counts in altered dark-BSE, and low counts in high-BSE areas whereas they did not show detectable variations among primary growth zone regions; (iii) Yttrium (Fig. 4a) and Al (Fig. 4c) show their highest concentrations in, or near, major fractures within the altered areas, with much lower count rates in the bulk of the altered areas. This suggests that non-formula elements were not homogeneously incorporated. Rather Y and Al might be assigned to the youngest fracture fillings, possibly representing a late stage of the ion exchange processes.

3.3. Effects of alteration on the U–Pb and Th–Pb isotopic systems

SHRIMP U–Th–Pb analysis results are listed in Table 2, along with birefringence, Raman band broadening, and BSE intensity data characterizing the analyzed micro-areas. Homogeneous high-BSE areas within the macro-porous zircon were too small for SHRIMP analysis, so only low-BSE areas within the macro-porous zircon were analyzed with the SHRIMP.

Almost one-half of the measured spots yielded highly discordant data in the U–Pb isotopic system (Table 2). Again, there is a clear correlation with the observed BSE intensities, and hence the alteration distribution within crystals; all low-BSE areas are normally discordant, plotting below the Concordia in Figure 5. A number of analyses in the zoned zircon yielded slight (mostly within the analytical uncertainty of measurements) reverse discordance; which may be either real or an analytical artifact. The SHRIMP analyses of high-uranium minerals such as zircon, monazite, or xenotime, often yield reversely discordant data with an apparent excess of Pb relative to U, especially in radiation-damaged regions in those minerals. This could be attributed to U loss (for instance due to ^{234}U ejection from porous zircon; Romer, 2003) or, less likely, to Pb gain (Williams et al., 1984). Alternatively, zircon decomposition into oxides may result in reversely discordant U–Pb data during SHRIMP analyses. This analytical artifact is produced by enhanced sputtering of Pb, which is preferentially incorporated into SiO_2, relative to U, which is preferentially incorporated in ZrO_2 (cf. McLaren et al., 1994). Williams and Hergt (2000) have identified a matrix affect on SHRIMP analyses where reverse discordance is correlated with U content in zircon with > 2000 ppm U. However, reversely discordant SHRIMP data is obviously not a general feature of U-rich zircon: Nasdala et al. (2002) obtained generally concordant U–Pb SHRIMP data for a highly metamict (amorphous), but unaltered, Sri Lankan gem zircon containing ~5,500 ppm of uranium.

It is most remarkable that the U–Pb data obtained within the zoned and the macro-porous zircon show the same general trend; all seem to plot near a discordia line that intersects Concordia at 1053 ± 11 and 266 ± 38 Ma [mean square weighted deviate (MSWD) = 9.2]. Separate evaluation of measurements within the two

textural types yielded intercepts at 1050 ± 12 and 251 ± 60 Ma (MSWD = 8.0) for the zoned and intercepts at 1058 ± 31 and 290 ± 62 Ma (MSWD = 8.0) for the macro-porous zircon, respectively, which are identical within error. The relevance of the calculated lower intercept age of 266 ± 38 Ma, however, should not be overestimated. We do not know whether the U–Pb disturbance is due to episodic Pb loss in the Permian to Early Mesozoic, or rather gradual young Pb leaching, or even multiple leaching events over a short time period after the initial closure of the U-Pb system (cf. Ashwal et al., 1999). There is no clear indication of recent Pb loss, as would be expected as a result of extensive incipient weathering (e.g., Compston et al., 1986; Black, 1987).

The nearly concordant Late Mesoproterozoic (Stenian) upper intercept age of 1050 ± 12 Ma of unaltered, light-BSE areas within the zoned zircon is likely to date primary zircon growth in an igneous environment, rather than complete U–Pb resetting. Given the slow diffusivity of Pb and U in crystalline zircon (i.e., volume diffusion) that does not have fast diffusion pathways, it is most unlikely that zircon with primary igneous zoning experienced complete U–Pb resetting at ~1050 Ma ago. The identical upper intercept age calculated within errors for the macro-porous zircon (1058 ± 31 Ma) is analogously assigned to the primary zircon growth. As discussed above, the boundary between macro-porous and zoned zircon is not always sharp but there may be a rather gradual transition (Fig. 1a). This seems to exclude the possibility that the macro-porous zircon represents inherited cores that were reset at the time of the igneous formation of the zoned zircon.

However, the age of when primary zircon was transformed into macro-porous zircon remains unclear. The assignment of this event appears most problematic; it can be accomplished in two ways, both of which involve a number of open questions. First, the transformation could also be assigned to the upper intercept age. This would indicate that the first alteration had occurred relatively shortly after primary growth, and that primary and alteration ages are similar and cannot be resolved by our U–Pb data. Second, the transformation could be assigned to a younger (i.e., Phanerozoic) event, possibly related to the (apparent) lower intercept age.

The first interpretation above is problematic as there are no obvious reasons for why, and how, only the central parts of crystals were reworked and transformed into the macro-porous zircon, whereas other parts were

not and retained their primary zoning. There exists the possibility that higher levels of incorporated trace elements, structural defects, and perhaps syn-genetic inclusions, may have made the central areas to some degree more susceptible to this alteration process. However, it remains doubtful why the central areas (which were virtually encapsulated by their surrounding zones) were well accessible to alteration fluids whereas the surrounding areas themselves remained unaffected. Note that notable fracturing of the surrounding zoned zircon at the time of the alteration, due to more extensive radiation damage in the central areas (Krogh and Davis, 1975), is unlikely if the alteration occurred shortly after zircon growth: In spite of comparably high U and Th concentrations on the order of 1 wt% and hence high self-irradiation rates, it would take at least several tens of millions of years to accumulate sufficient radiation damage to cause fracturing of less metamict zones (cf. Chakoumakos et al., 1987; Lee and Tromp, 1995).

The second interpretation above (in which the alteration is much younger than the upper intercept age) is also problematic as it appears unlikely that the majority of the radiogenic Pb has been retained during a fluid-driven replacement reaction that virtually completely erased the primary zoning during major textural reworking. On the other hand, it is well known that zircon affected by alteration processes may incorporate unusually high concentrations of common Pb (Corfu, 1987; Mathieu et al., 2001; Nasdala et al., 2009). We therefore cannot exclude the hypothetical possibility that the Saranac Prospect zircon may have undergone low-*T* alteration without notable loss of its radiogenic Pb. The assignment of the formation of the macro-porous zircon to a younger event would agree well with earlier interpretations (Krogh and Davis, 1975; rediscussed in Lumpkin, 2001) according to which the central, reworked areas were preferentially altered after having accumulated elevated levels of radiation damage, by fluids assessing though fractures in their surrounding zircon zones.

Alteration within the zoned zircon is clearly controlled by the accessibility of the alteration fluids through fractures (Figs. 2c, d) that formed by heterogeneous volume expansion resulting from heterogeneous self-irradiation. This second alteration process therefore must have occurred a significant time period after the primary zircon growth.

3.4. Self-irradiation damage

Most parts of the zircon crystals are characterized by remarkably low (i.e., 1st order gray) interference colors, or optical isotropy indicated by no interference at all (Fig. 1). Such interference colors correspond to birefringence values in the range 0.000–0.010 (Table 2). Only a small fraction of zones within the zoned interior region, in particular the outermost growth zones at pyramid faces (see Fig. 1a, tip of right crystal), show 2nd order to low 3rd order interference colors, corresponding to birefringence values up to ~0.040. However, even the latter value is well below the birefringence of well-crystallized zircon (0.059; Tröger, 1982). The low birefringence is assigned to generally high levels of accumulated radiation damage, which is connected with the loss of anisotropy (cf. Morgan and Auer, 1941; Sahama, 1981; Chakoumakos et al., 1987).

This assignment is supported by Raman analyses of the Saranac Prospect zircon crystals. In zones with the highest interference colors, the main internal SiO_4 vibration (ν_3, anti-symmetric stretching; Dawson et al., 1971) was found to have a FWHM of 14–18 cm^{-1}. Zones and areas with 1st order gray interference color yielded low-intensity, asymmetric Raman bands with FWHMs exceeding 30 cm^{-1} (Table 2). In zones that did not show interference colors at all (Fig. 1a), no Raman bands of crystalline zircon were detected; this is assigned to an almost complete metamictization of these zones. The observed general relation between Raman band FWHMs and birefringence values (Table 2) corresponds well to the relation described by Palenik et al. (2003).

The time-integrated alpha fluences listed in Table 2 were calculated for self-irradiation periods matching the calculated upper and lower intercept ages on the Concordia plot. The observed degrees of radiation damage (estimated from Raman band FWHMs and birefringence) are clearly higher than it would correspond to self-irradiation over a 266 myr period (Fig. 6). For instance, zircon micro-areas that have experienced $3–6 \times 10^{15}$ alpha-decay events per mg of material should be expected to be moderately damaged, with birefringence higher than ≥0.020 (compare Equation 3 and Fig. 3 of Palenik et al., 2003), whereas the measured birefringence values

are ≤0.004, indicating strong radiation damage (Table 2). Also, zircon that has experienced less than 1×10^{15} alpha-decay events per mg (cf. analyses 8 and 12 in Table 2) should yield $\nu_3(SiO_4)$ Raman band FWHMs smaller than 8 cm^{-1} (Nasdala et al., 2001) whereas much wider bands (14–25 cm^{-1}) were observed (Table 2; white circles in Fig. 6). Consequently, 266 myr alpha doses clearly underestimate the amount of radiation damage that is currently present. This observation indicates that the Saranac Prospect zircon cannot have experienced major structural reconstitution through thermal annealing of the previously existing radiation damage at Late Paleozoic times. On the other hand, the three SHRIMP spots in the un-altered, zoned zircon with the lowest degree of radiation damage (black circles in Fig. 6) are less radiation-damaged than it would correspond to complete damage accumulation since the time of crystal growth, indicating moderate post-growth thermal annealing. We conclude that Pb loss (and perhaps the second chemical alteration) must have occurred at low *T*, probably well below 200 °C. This estimate is based on results of Weber et al. (1994, 1997) and Meldrum et al. (1999) who predicted that long-term annealing of alpha-event damage is expected at temperatures as low as 150–200 °C.

3.5. Further discussion

The chemical and physical alteration of the Saranac Prospect zircon was affected by two factors. First, the alteration was controlled by the accessibility of volume areas to the transporting phase, i.e., hydrothermal fluids. Consequently, initial alteration during this phase is characterized by finger-like patterns along large fractures that have served as “fast pathways” (Figs. 2a–d). Also, alteration appears to be especially intense in the macro-porous zircon whose porosity may have aid circulation of the fluid. The crucial role of pathways is also indicated by varying degrees of U–Th–Pb isotopic discordance: The extent of secondary Pb loss is highly variable and it appears reasonable to speculate that Pb loss was strongly affected by the presence of migration pathways. Second, there are clear effects of the radiation damage. Near large fractures cross-cutting several growth zones, mostly the higher-U, more radiation-damaged zones are preferentially altered whereas the lower

U, and less radiation-damaged zones, remained virtually unaffected (Figs. 2c, e, and f). Even though potential effects of variations of the chemical composition on the susceptibility of zircon to dissolution cannot be neglected, we interpret the different degrees of radiation damage among growth zones, resulting from varying initial U and Th concentrations, as the main reason for the different behavior among zones. This agrees very well with the conclusions in Davis and Krogh (2000) and Lumpkin (2001) who have assigned fluid-driven alteration to metamictization and concluded that chemical control alone was insignificant. We did not find clear evidence for strain or other effects of mechanical deformation (cf. Timms et al., 2006) affecting the leaching and U retention properties of zircon.

The observations made in the present study correspond well to findings of Lee (1993) who discussed that radiation damage alone does not cause U–Th–Pb isotopic discordance through Pb loss from zircon; rather element and fluid transport along major pathways and chemical leaching are the two dominant cation exchange processes in radiation-damaged minerals. The observation that high-BSE areas in the Saranac Prospect zircon are (close to) concordant, even though being highly radiation-damaged, whereas intensely altered, low-BSE areas tend to have experienced notable Pb loss, suggests that a fluid-driven ion-exchange reaction either causes Pb loss, or strongly enhances the susceptibility of zircon to the subsequent loss of the radiogenic Pb (cf. Krogh and Davis, 1973; 1975).

In contrast to strong variations in radiogenic Pb, the primary U that was incorporated in the zircon structure has remained only mildly affected by the replacement reaction. This is clearly observable if the chemical analyses placed in unaltered and altered regions of the very same growth zone are compared (see zones B, C, D, E, G. H, I, and J in Table 1). The ratios between the content in an altered area and its unaltered counterpart was found to vary in the range 0.87–0.98 (average 0.95 ± 0.04) for ZrO_2, 0.92–0.98 (average 0.95 ± 0.02) for SiO_2, and 0.76–1.16 (average 0.94 ± 0.14) for UO_2, respectively. These average ratios reflect the typical moderate loss of chemical constituents in fluid-driven replacement reactions (cf. Putnis, 2002). Most remarkably, however, is the observation that the U loss is within errors identical to the losses of Zr and Si. The chemical alteration these zircon crystals have experienced, has clearly not resulted in preferential leaching of U;

rather Zr, Si, and U have been uniformly incorporated in the newly formed zircon. The latter is also strikingly apparent in the preservation of primary U zoning in alteration-overprinted areas (see U distribution maps in Figs. 4a, b). In summary, the multiple, low-*T* chemical alteration of the Saranac Prospect zircon has finally resulted in highly variable loss, of up to 80%, of the radiogenic Pb accumulated since primary crystallization and prior to the last closure of the U-Pb system (cf. again Table 2) whereas there were only minor U losses.

4. Conclusions

If zircon is in the presence of chemically aggressive hydrothermal fluids, for extended periods of time, then an essential question to answer (with regard to both its use in geochronology or as a potential nuclear waste repository material) is, to what degree the radionuclides are preferentially removed? In the present study, we show with the example of naturally altered zircon crystals from Bancroft, Ontario, that extensive low-*T* chemical replacement does not necessarily result in preferential leaching of U from strongly radiation-damaged zircon. This seems to question the general relevance of hydrothermal treatment experiments to a reliable assessment of the (self-irradiation dependent) long-term behavior of zircon and other actinide host materials under moderately “wet”, low-*T* environmental conditions. The finding that zircon, under certain environmental conditions, has high ability to retain its trace uranium, might affect the interpretation of radiometric dating results, in particular discussions of possible causes of U–Pb discordance. Second, observations suggest that zircon, and even radiation-damaged zircon, may be a suitable ceramic waste form for the long-term immobilization and storage of radionuclides.

Acknowledgments

The SHRIMP II ion microprobe used in this study is operated by a consortium consisting of Curtin University of Technology, the University of Western Australia, and the Geological Survey of Western Australia. The SHRIMP reference zircon M257 was made available by W. Hofmeister (Institute of Gemstone Research, Idar-Oberstein and Mainz, Germany). We are indebted to D. Moser (University of Western Ontario, London) for providing the original zircon sample to J.M.H. in 1997, and to Robert Ramik (Royal Ontario Museum, Toronto), for providing additional information on the zircon sample and its origin. We thank A. Wagner (Universität Wien) for sample preparation, K. Ruschel and E. Libowitzky (both Universität Wien), for experimental assistance, and D.W. Davis (University of Toronto), for constructive discussions. Also, we are grateful to two anonymous reviewers and associate editor B. Bourdon for helpful comments. Financial support was provided by the European Commission trough contract no. MEXC-CT-2005-024878 and the Austrian Science Fund (FWF), grant P20028-N10, to L.N.

References

Armstrong, J.T., 1995. CITZAF: A package of correction programs for the quantitative electron microbeam X-ray analysis of thick polished materials, thin films, and particles. Microbeam Analysis 4, 177–200.

Ashwal, L.D., Tucker, R.D., Zinner, E.K., 1999. Slow cooling of deep crustal granulites and Pb-loss in zircon. Geochimica et Cosmochimica Acta 63, 2839–2851.

Black, L.P., 1987. Recent Pb loss in zircon: a natural or laboratory-induced phenomenon? Chemical Geology (Isotope geoscience Section) 65, 25–33.

Breiter, K., Förster, H.-J., Škoda, R., 2006. Extreme P-, Bi-, Nb-, Sc-, U- and F-rich zircon from fractionated perphosphorous granites: The peraluminous Podlesí granite system, Czech Republic. Lithos 88, 15–34.

Caruba, R., Mano, J., Dors, R., Turco, G, 1974. Corrosions expérimentales de critaux de zircons et comparaison avec des corrosions naturelles de zircons de granites albitisés. Tschermaks Mineralogische und Petrologische Mitteilungen 21, 33–46.

Chakoumakos, B.C., Murakami, T., Lumpkin, G.R., Ewing, R.C., 1987. Alpha-decay-induced fracturing in zircon: The transition from the crystalline to the metamict state. Science 236, 1556–1559.

Cherniak, D.J., Watson, E.B., 2001. Pb diffusion in zircon. Chemical Geology 172, 5–24.

Cherniak, D.J., Watson, E.B., 2003. Diffusion in zircon. In: Hanchar, J.M., Hoskin, P.W.O (Eds.), Zircon. Reviews in Mineralogy and Geochemistry 53, Mineralogical Society of America, Washington, DC., pp. 113–143.

Compston, W., Williams, I.S., Meyer, C., 1984. U–Pb geochronology of zircon from lunar breccia 73217 using a sensitive high mass-resolution ion microprobe, Journal of Geophysical Resources 89, 525–534.

Compston, W., Kinny, P.D., Williams, I.S., Foster, J.J., 1986. The age and Pb loss behaviour of zircons from the Isua supracrustal belt as determined by ion microprobe. Earth and Planetary Science Letters 80, 71–81.

Connelly J.N., 2000. Degree of preservation of igneous zonation in zircon as a signpost for concordancy in U/Pb geochronology. Chemical Geology 172, 25–39.

Corfu, F., 1987. Inverse age stratification in the archaean crust of the superior province: Evidence for infra- and subcrustal accretion from high resolution U-Pb zircon and monazite ages. Precambrian Research 36, 259–275.

Corfu, F., Hanchar, J.M., Hoskin, P.W.O., Kinny, P., 2003. Atlas of zircon textures. In: Hanchar, J.M., Hoskin, P.W.O (Eds.), Zircon. Reviews in Mineralogy and Geochemistry 53, Mineralogical Society of America, Washington, DC., pp. 469–500.

Davis, D.W., Krogh, T.E., 2000. Preferential dissolution of ^{234}U and radiogenic Pb from α-recoil-damaged lattice sites in zircon: implications for thermal histories and Pb isotopic fractionation in the near surface environment. Chemical Geology 172, 41–58.

Davis, D.W., Williams, I.S., Krogh, T.E., 2003. Historical development of zircon geochronology. In: Hanchar, J.M., Hoskin, P.W.O (Eds.), Zircon. Reviews in Mineralogy and Geochemistry 53, Mineralogical Society of America, Washington, DC., pp. 145–181.

Dawson, P., Hargreave, M.M., Wilkinson, G.R.,1971. The vibrational spectrum of zircon ($ZrSiO_4$). Journal of Physics C: Solid State Physics 4, 240–256.

De Laeter, J.R., Kennedy, A.K., 1998. A double focussing mass spectrometer for geochronology. International Journal of Mass Spectrometry and Ion Processes 178, 43–50.

Ewing, R.C., 1994. The metamict state: 1993 – the centennial. Nuclear Instruments and Methods in Physics Research Section B: Beam Interactions with Materials and Atoms 91, 22–29.

Ewing, R.C., 1999. Nuclear waste form for actinides. Proceedings of the National Academy of Sciences of the United States of America 96, 3432–3439.

Ewing, R.C., 2001. The design and evaluation of nuclear-waste forms: Clues from mineralogy. Canadian Mineralogist 39, 697–715.

Ewing, R.C., Meldrum, A., Wang, L., Weber, W.J., Corrales, L.R., 2003. Radiation effects in zircon. In: Hanchar, J.M., Hoskin, P.W.O (Eds.), Zircon. Reviews in Mineralogy and Geochemistry 53, Mineralogical Society of America, Washington, DC., pp. 387–425.

Geisler, T., Pidgeon, R.T., von Bronswijk, W., Kurtz, R., 2002. Transport of uranium, thorium, and lead in metamict zircon under low-temperature hydrothermal conditions. Chemcial Geology 191, 141–154.

Geisler,T., Rashwan, A.A., Rahn, M.K.W., Poller, U., Zwingmann, H., Pidgeon, R.T., Schleicher, H., Tomaschek, F., 2003a. Low-temperature hydrothermal alteration of natural metamict zircon from the Eastern Desert, Egypt. Mineralogical Magazine 67, 485–508.

Geisler,T., Schleicher, H., Kurtz, R., van Bronswijk, W., Schleicher, H., 2003b. Experimental hydrothermal alteration of partially metamict zircon. American Mineralogist 88, 1496–1513.

Gentry, R.V., Sworski, T.J., Mckown, H.S., Smith, D.H., Eby, R.E., Christie, W.H., 1982. Differential lead retention in zircons: implications for nuclear waste containment. Science 216, 296–298.

Hansen, B.T., Friderichsen, J.D., 1989. The influence of recent lead loss on the interpretation of disturbed U-Pb systems in zircons from igneous rocks in East Greenland. Lithos 23, 209–223.

Hoskin, P.W.O., 2000. Patterns of chaos: Fractal statistics and the oscillatory chemistry of zircon. Geochimica et Cosmochimica Acta 64, 1905–1923.

Jaffey, A.H., Flynn, K.F., Glendenin, L.E., Bentley, W.C., Essling, A.M., 1971. Precision measurement of half-lives and specific activities of ^{235}U and ^{238}U. Physical Review C 4, 1889–1906.

Johan, Z., Johan, V., 2005. Accessory minerals of the Cínovec (Zinnwald) granite cupola, Czech Republic: indicators of petrogenetic evolution. Mineral. Petrol. 83, 113–150.

Keller L.M., Wirth, R., Rhede, D., Kunze, K., Abart, R., 2008. Asymmetrically zoned reaction rims: assessment of grain boundary diffusivities and growth rates related to natural diffusion-controlled mineral reactions. Journal of Metamorphic Geology 26, 99–120.

Krogh, T.E., 1993. High precision U-Pb ages for granulite metamorphism and deformation in the Archean Kapuskasing structural zone, Ontario: implications for structure and development of the lower crust. Earth and Planetary Science Letters 119, 1–18.

Krogh, T.E., Davis, G.L., 1973. Alteration in zircons with discordant U-Pb ages. Year book / Carnegie Institution of Washington 73, 560–567.

Krogh, T.E., Davis, G.L., 1975. Alteration in zircons and differential dissolution of altered and metamict zircon. Year book / Carnegie Institution of Washington 74, 619–623.

Labotka, T.C., Cole, D.R., Fayek, M., Riciputi, L.R., Stadermann, F.J., 2004. Coupled cation and oxygen-isotope exchange between alkali feldspar and aqueous chloride solution. American Mineralogist 89, 1822–1825.

Lakis, R., Lyman, C., Goldstein, J., 1992. Electron-probe microanalysis of porous materials. In: 50th Annual Meeting of the Electron Microscopy Society of America. Proceedings. 1660–1661.

Lee, J.K.W., 1993. Problems and progress in the elucidation of U and Pb transport mechanisms in zircon. In: Boland, J.N., Fitz Gerald, J.D. (Eds.), Defects and processes in the solid state: Geoscience applications. The McLaren volume. Elsevier, pp 423–446.

Lee, J.K.W., Tromp, J., 1995. Self-induced fracture generation in zircon. Journal of Geophysical Research - Solid Earth 100, 17753–17770.

Ludwig, K.R., 2002. SQUID 1.02, a user's manual. Berkeley Geochronology Center Special Publication 2, 22 p.

Ludwig, K.R., 2003. User’s manual for Isoplot 3.00: A geochronological toolkit for Microsoft Excel. Berkeley Geochronology Center Special Publication 4, 71 p.

Lumpkin, G.R., 2001. Alpha-decay damage and aqueous durability of actinide host phases in natural systems. Journal of Nuclear Materials 289, 136–166.

Lumpkin, G.R., 2006. Ceramic waste forms from actinides. Elements 2, 365–372.

Mathieu, R., Zetterström, L., Cuney, M., Gauthier-Lafaye, F., Hidaka, H., 2001. Alteration of monazite and zircon and lead migration as geochemical tracers of fluid paleocirculations around the Oklo–Okélobondo and Bangombé natural nuclear reaction zones (Franceville basin, Gabon). Chemical Geology 171, 147–171.

Mattinson, J.M., 1994. A study of complex discordance in zircons using step-wise dissolution techniques. Contributions to Mineralogy and Petrology 116, 117–129.

Mattinson, J.M., 2005. Zircon U–Pb chemical abrasion ("CA-TIMS") method: Combined annealing and multi-step partial dissolution analysis for improved precision and accuracy of zircon ages. Chemical Geology 220, 47–66.

McLaren, A.C., Fitz Gerald, J.D., Williams, I.S., 1994. The microstructure of zircon and its influence on the age determination from Pb/U isotopic ratios measured by ion microprobe. Geochimica et Cosmochimica Acta 58, 993–1005.

Meldrum, A., Boatner, L.A., Zinkle, S.J., Wang, S.-X., Wang, L.-M., Ewing, R.C., 1999. Effects of dose rate and temperature on the crystalline-to-metamict transformation in the ABO_4 orthosilicates. Canadian Mineralogist 37, 207–221.

Morgan, J.H., Auer, M.L., 1941. Optical, spectrographic, and radio-activity studies of zircon. American Journal of Science 239, 305–311.

Murakami, T., Chakoumakos, B.C., Ewing, R.C., Lumpkin, G.R., Weber, W.J., 1991. Alpha-decay event damage in zircon. American Mineralogist 76, 1510–1532.

Nasdala, L., Irmer, G., Wolf, D., 1995. The degree of metamictization in zircon: a Raman spectroscopic study. European Journal of Mineralogy 7, 471–478.

Nasdala, L., Wenzel, T., Pidgeon, R.T., Kronz, A., 1999. Internal structures and dating of complex zircons from Meissen Massif monzonites, Saxony. Chemical Geology 156, 331–341.

Nasdala, L., Wenzel, M., Vavra, G., Irmer, G., Wenzel, T., Kober, B., 2001. Metamictisation of natural zircon: Accumulation versus thermal annealing of radioactivity-induced damage. Contributions to Mineralogy and Petrology 141, 125–144.

Nasdala, L., Lengauer, C.L., Hanchar, J.M., Kronz, A., Wirth, R., Blanc, P., Kennedy, A.K., Seydoux-Guillaume, A.-M., 2002. Annealing radiation damage and the recovery of cathodoluminescence. Chemical Geology 191, 121–140.

Nasdala, L., Hanchar, J.M., Kronz, A., Whitehouse, M.J., 2005. Long-term stability of alpha particle damage in natural zircon. Chemical Geology 220, 83–103.

Nasdala, L., Hofmeister, W., Norberg, N., Mattinson, J.M., Corfu, F., Dörr, W., Kamo, S.L., Kennedy, A.K., Kronz, A., Reiners, P.W., Frei, D., Kosler, J., Wan, Y., Götze, J., Häger T., Kröner, A., Valley, J.W., 2008. Zircon M257 - a homogeneous natural reference material for the ion microprobe U-Pb analysis of zircon. Geostandards and Geoanalytical Research 32, 247–265.

Nasdala, L., Kronz, A., Wirth, R., Váczi, T., Pérez-Soba, C., Willner, A., Kennedy, A.K., 2009. Alteration of radiation-damaged zircon and the related phenomenon of deficient electron microprobe totals. Geochimica et Cosmochimica Acta 73, 1637–1650.

Palenik, C.S., Nasdala, L., Ewing, R.C., 2003. Radiation damage in zircon. American Mineralogist 88, 770–781.

Pérez-Soba, C., Villaseca, C., Gonzáles del Tánago, J., Nasdala, L., 2007. The composition of zircon in the peraluminous Hercynian granites of the Spanish Central System batholith. Canadian Mineralogist 45, 509–527.

Peterman, Z.E., Zartman, R.E., Sims, P.K., 1986. A protracted Archean history in the Watersmeet gneiss dome, northern Michigan. U.S. Geological Survey Bulletin 1622, 51–64.

Pidgeon, R.T., O'Neil, J.R., Silver, L.T., 1966. Uranium and lead isotope stability in a metamict zircon under experimental hydrothermal conditions. Science 154, 1538–1540.

Pointer, C.M., Ashworth, J.R., Ixer, R.A., 1988. The zircon-thorite mineral group in metasomatized granite, Ririwai, Nigeria. 2. Zoning, alteration and exsolution in zircon. Mineralogy and Petrology 39, 21–37.

Pöml, P., Meneken, M., Stephan, T., Niedermeier, D.R.D., Geisler, T., Putnis, A., 2007. Mechanism of hydrothermal alteration of natural self-irradiated and synthetic crystalline titanate-based pyrochlore. Geochimica et Cosmochimica Acta 71, 3311–3322.

Prasad, E.A.V., Naidu, M.G.C., 1971. Leaching patterns of monazite and zircon. Current Science 40, 14–15.

Putnis, A., 2002. Mineral replacement reactions: from macroscopic observations to microscopic mechanisms. Mineralogical Magazine 66, 689–708.

Putnis, C., Geisler, T., Schmid-Beurmann, P., Stephan, T., Giampaolo, C, 2007. An experimental study of the replacement of leucite by analcime. American Mineralogist 92, 19–26.

Rimša, A., Whitehouse, M.J., Johansson, L., Piazolo, S., 2007. Brittle fracturing and fracture healing of zircon: An integrated cathodoluminescence, EBSD, U-Th-Pb, and REE study. American Mineralogist 92, 1213–1224.

Rizvanova, N.G., Levchenkov, O.A., Belous, A.E., Bezmen, N.I., Maslenikov, A.V., Komarov, A.N., Makeev, A.F., Levskiy, L.K., 2000. Zircon reaction and stability of the U-Pb isotope system during interaction with carbonate fluid: experimental hydrothermal study. Contributions to Mineralogy and Petrology 139, 101–114.

Romer, R.L., 2003. Alpha-recoil in U-Pb geochronology: effective sample size matters. Contributions to Mineralogy and Petrology 145, 481–491.

Sahama, T.G., 1981. Growth structure in Ceylon zircon. Bulletin de Minéralogie 104, 89–94.

Satterly, J., 1957. Radioactive mineral occurrences in the Bancroft area. Ontario Department of Mines, Annual Report 1956, 65 (part 6), 108–115.

Schoene B., Crowley J.L., Condon D.J., Schmitz M.D., Bowring S.A., 2006. Reassessing the uranium decay constants for geochronology using ID-TIMS U-Pb data. Geochimica et Cosmochimica Acta 70, 426–445.

Shukolyukov, Yu.A., Prevdivtseva, A.V., Kotov, N.V., 1994. The U-Pb and U-Xe isotope systems in metamict zircons at elevated T and P. Geochemistry International 31, 65–72.

Sinha, A.K., Wayne, D.W., Hewitt, D.A., 1992. The hydrothermal stability of zircon: Preliminary experimental and isotopic studies. Geochimica et Cosmochimica Acta 56, 3551–3560.

Sláma, J., Košler, J, Condon, D.J., Crowley, J.L., Gerdes, A., Hanchar, J.M., Horstwood, M.S.A., Morris, G.A., Nasdala, L., Norberg, N., Schaltegger, U., Tubrett, M.N., Whitehouse, M.J., 2008. Plešovice zircon – a new natural reference material for U-Pb and Hf isotopic microanalysis. Chemical Geology 249, 1–35.

Smith, D.G.W., de St. Jorre, L., Reed, S.J.B., Long, J.V.P., 1991. Zonally metamictized and other zircons from Thor Lake, Northwest Territories. Canadian Mineralogist 29, 301–309.

Sorbier, L., Rosenberg, E., Merlet, C., 2004. Microanalysis of porous materials. Microscopy and Microanalysis 10, 745–752.

Timms, N.E., Kinny, P.D., Reddy, S.M., 2006. Enhanced diffusion of uranium and thorium linked to crystal plasticity in zircon. Geochemical Transactions 7, 10.

Tole, M.P., 1985. The kinetics of dissolution of zircon ($ZrSiO_4$). Geochimica et Cosmochimica Acta 49, 453–458.

Tomaschek, F., Kennedy, A.K., Villa, I.M., Lagos, M, Ballhaus, C., 2003. Zircons from Syros, Cyclades, Greece – Recrystallization and mobilization of zircon during high-pressure metamorphism. Journal of Petrology 44, 1977–2002.

Törnroos, R., 1985. Metamict zircon from Mozambique. Bulletin of the Geological Society of Finland 57, 181–195.

Tröger, W.E., 1982. Optical determination of rock-forming minerals. I. Determinative tables. E. Schweitzerbart'sche Verlagsbuchhandlung, Stuttgart, 188 p.

Utsunomiya, S., Valley, J.W., Cavosie, A.J., Wilde, S.A., Ewing, R.C., 2007. Radiation damage and alteration of zircon from a 3.3 Ga porphyritic granite from the Jack Hills, Western Australia. Chemical Geology 236, 92–111.

Van Lichtervelde, M., Melcher, F., Wirth, R., 2009. Magmatic vs. hydrothermal origins for zircon associated with tantalum mineralization in the Tanco pegmatite, Manitoba, Canada. American Mineralogist 94, 439–450.

Weber, W.J., Ewing, R.C., Wang, L.-M., 1994. The radiation-induced crystalline-to-amorphous transition in zircon. Journal of Materials Research 9, 688–698.

Weber, W.J., Ewing, R.C., Meldrum, A., 1997. The kinetics of alpha-decay-induced amorphization in zircon and apatite containing weapons-grade plutonium or other actinides. Journal of Nuclear Materials 250, 147–155.

Weber, W.J., Ewing, R.C., Catlow, C.R.A., Diaz de la Rubia, T., Hobbs, L.W., Kinoshita, C., Matzke, H., Motta, A.T., Nastasi, M., Salje, E.K.H., Vance, E.R., Zinkle, S.J., 1998. Radiation effects in crystalline ceramics for the immobilization of high-level nuclear waste and plutonium. Journal of Materials Research 13, 1434–1484.

Williams, I.S., Compston, W., Black, L.P., Ireland, T.R., Foster, J.J., 1984. Unsupported radiogenic Pb in zircon: a cause of anomalously high Pb-Pb, U-Pb and Th-Pb ages. Contributions to Mineralogy and Petrology 88, 322–327.

Williams, I.S., Hergt, J.M., 2000. U-Pb dating of Tasmanian dolerites: a cautionary tale of SHRIMP analysis of high U zircon. In: Woodhead, J.D., Hergt, J.M., Noble, W.P. (Eds.), Beyond 2000: New frontiers in isotope geoscience, Lorne, Australia. Abstracts and Proceedings, pp. 185–188.

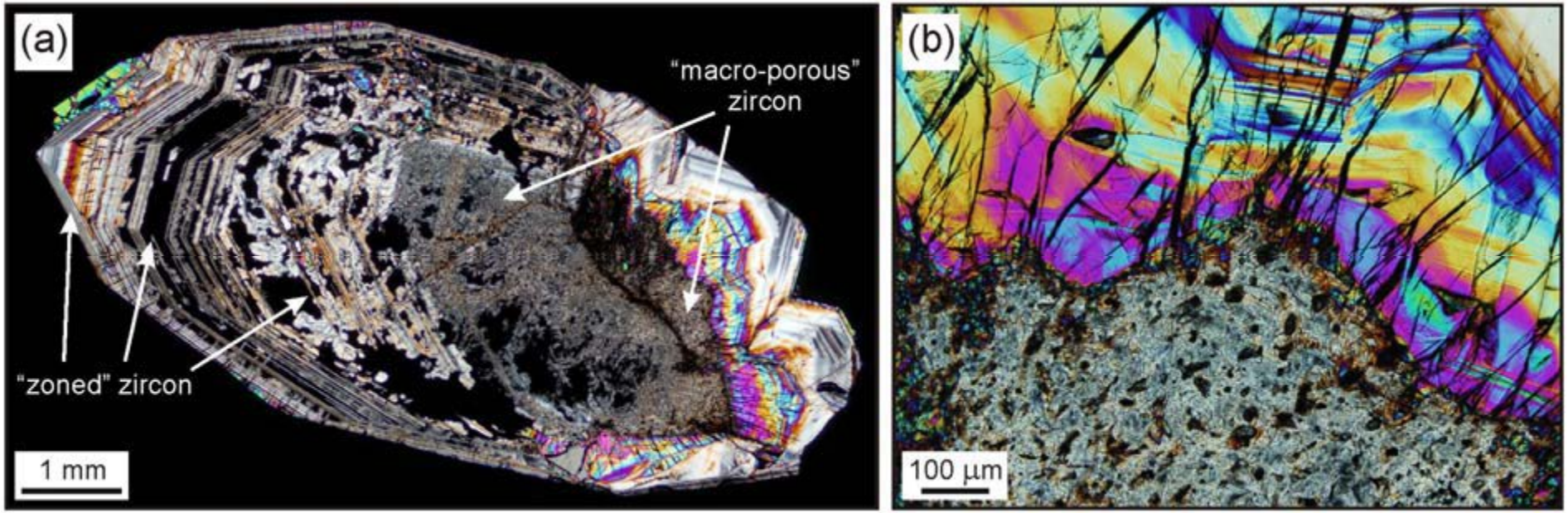

Fig. 1. Photomicrograph (cross-polarized light) of a large, heterogeneous zircon crystal from the Saranac prospect (a), and close-up of the sharp boundary between the "macro-porous" and "zoned" interior regions (b).

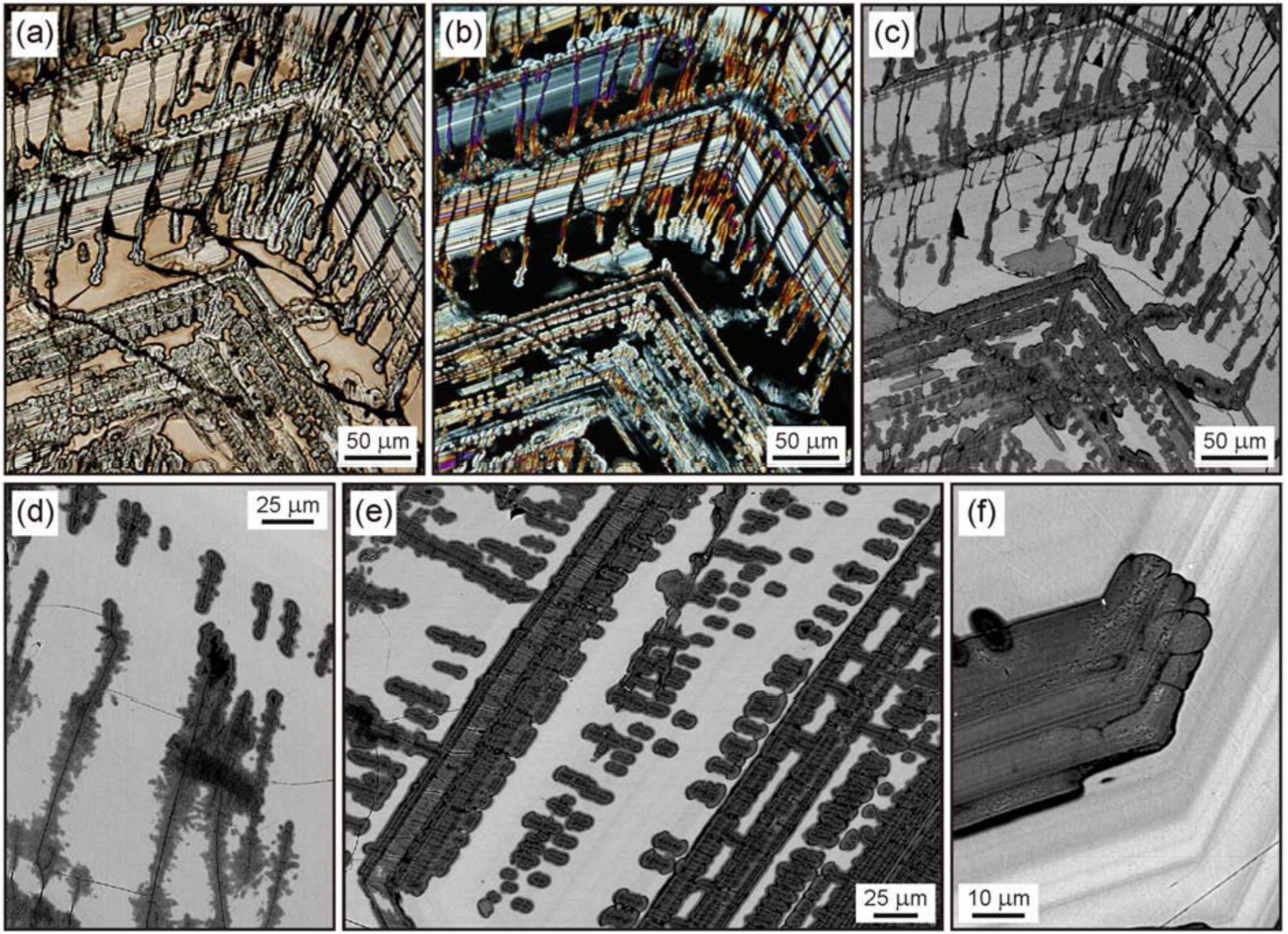
(a)
50 µm
(b)
50 µm
(c)
50 µm
(d)
25 µm
(e)
25 µm
(f)
10 µm

Fig. 2. Images of the “zoned” zircon. Series of plane-polarized (a) and cross-polarized photomicrographs (b) and BSE image (c) of a partially altered region. Altered micro-areas that emanate from fractures have a finger-like appearance, are virtually de-colored, and show enhanced birefringence and darker BSE intensity compared to neighboring areas of the same growth zones. (d) BSE image showing alteration emanating from large fractures. (e) BSE image of an intensely altered area. Alteration had followed the primary growth zoning. (f) Close-up showing that the primary zoning is still preserved in the altered material (dark BSE), which is characterized by sub-micrometer range porosity (center of image).

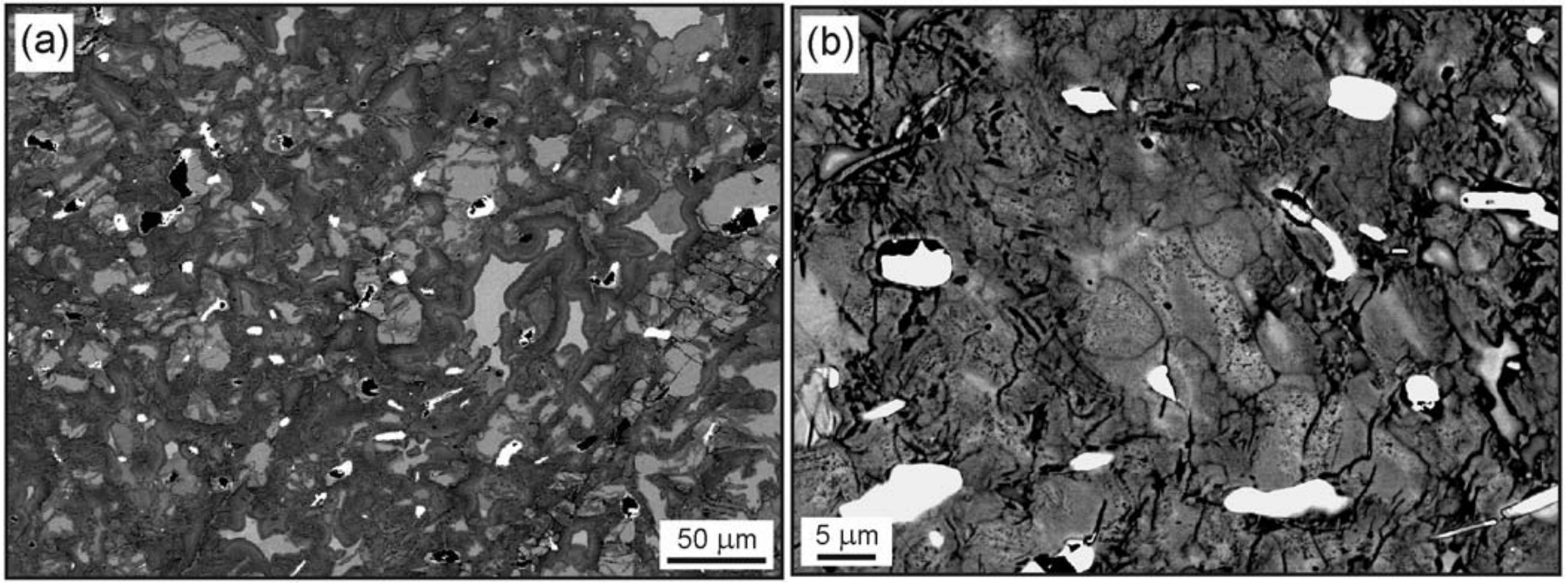

Fig. 3. Two BSE images of the „macro-porous“ zircon (a) A large volume fraction of the zircon is characterized by dark BSE. This material is rich in inclusions with high average atomic number (bright) and pres (black) with sizes up to several tens of micrometers (b) Close up showing additional sub-micrometer porosity (center of image.)

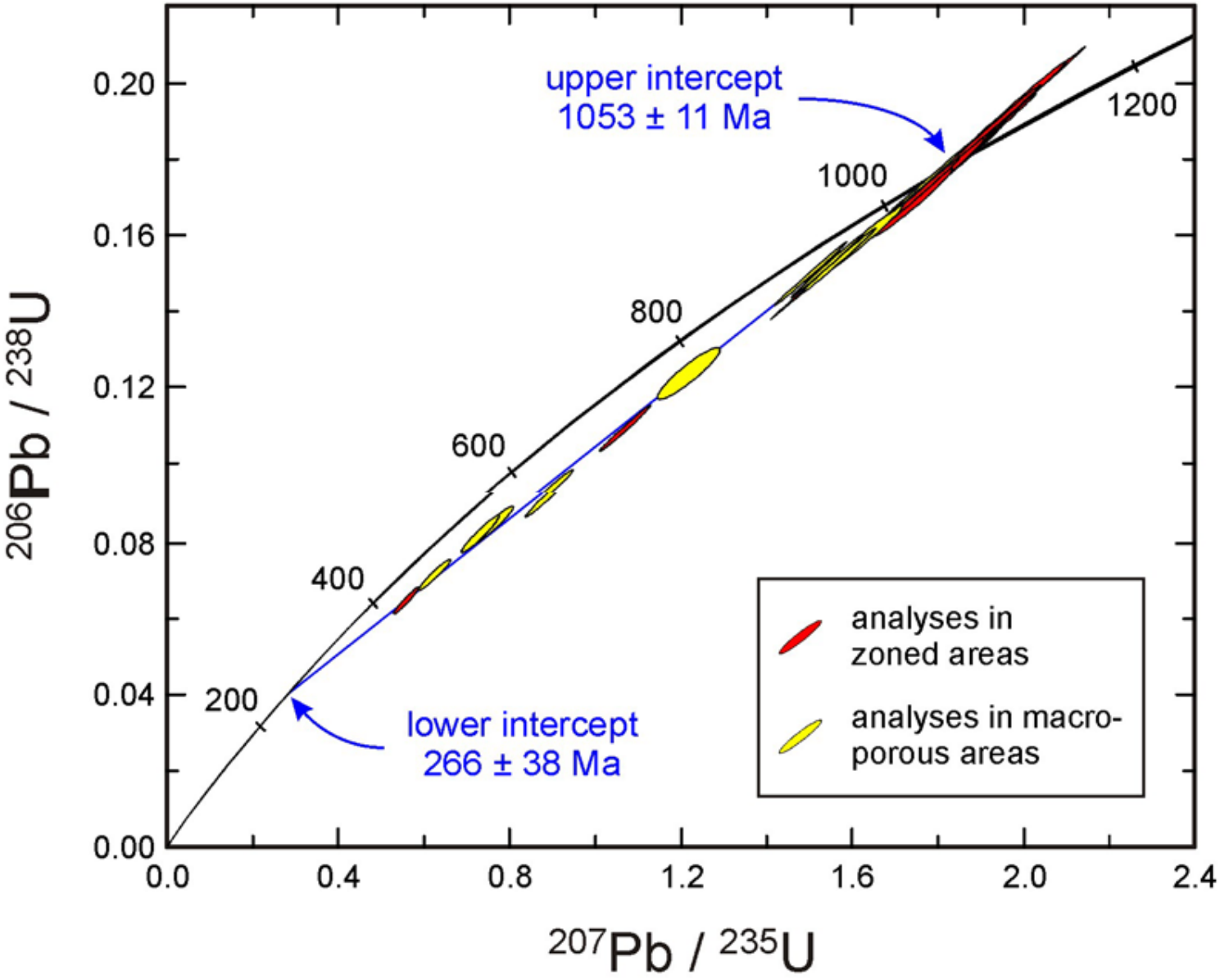

Fig. 4. Results of SHRIMP U-Pb analysis. Error ellipses represent 2 σ uncertainties

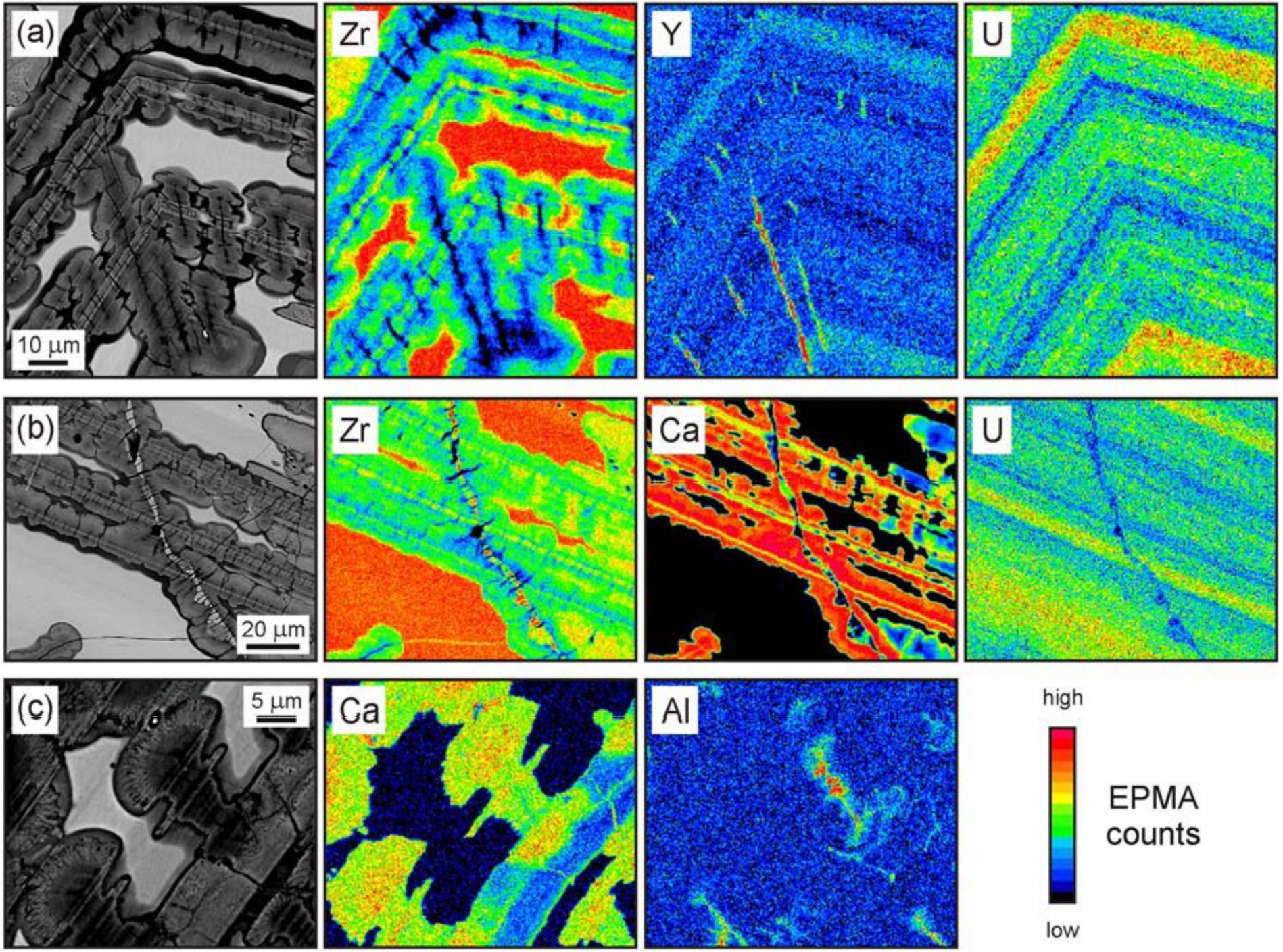
(a)
Zr
Y
U
10 µm
(b)
Zr
Ca
U
20 µm
(c)
5 µm
Ca
Al
high
low
EPMA
counts

Fig. 5. Three series of EMPA element maps along with the corresponding BSE patterns, obtained in heavily altered areas within the "zoned" zircon. Color-coded count rate ranges are: upper row (15 kV, 4×10^{-8} A, dwell time 1500 ms), 9,880−12,262 (Zr), 2−44 (Y), 27−107 (U); middle row (15 kV, 1×10^{-8} A, dwell time 1000 ms), 3,500−4,855 (Zr), 226−1,333 (Ca), 5−50 (U); lower row (6 kV, 1×10^{-8} A, dwell time 1000 ms), 6−79 (Ca), 1−35 (Al).

Table 1. Results of EMPA chemical analyses (wt%).

Analysis no.	Zone*	BSE intensity	Al_2O_3	SiO_2	CaO	FeO	Y_2O_3	ZrO_2	Yb_2O_3	HfO_2	PbO	ThO_2	UO_2	Total
Analyses in "zoned" interior regions:														
1	A	high	(bdl)	33.6	(bdl)	(bdl)	(bdl)	65.1	(bdl)	0.79	0.02	0.03	0.20	100.2
2	A	high	(bdl)	33.6	(bdl)	(bdl)	0.13	65.0	(bdl)	1.24	0.03	0.02	0.22	100.6
3	B	high	(bdl)	33.4	(bdl)	(bdl)	0.16	64.9	(bdl)	0.88	0.04	0.03	0.35	100.2
4	B	high	(bdl)	32.2	(bdl)	(bdl)	0.21	65.4	(bdl)	0.99	0.08	0.02	0.39	99.9
5	B	low	0.09	30.4	2.89	0.58	0.14	60.6	(bdl)	1.23	(bdl)	(bdl)	0.32	96.6
6	C	high	(bdl)	32.0	(bdl)	(bdl)	0.15	64.8	(bdl)	0.37	0.08	0.05	0.54	98.3
7	C	low	0.91	30.7	3.07	0.70	0.79	56.2	(bdl)	0.69	(bdl)	0.03	0.45	94.7
8	D	high	(bdl)	32.2	(bdl)	(bdl)	0.24	65.1	(bdl)	1.01	0.05	0.03	0.42	99.6
9	D	low	0.12	30.2	3.10	0.60	0.22	60.1	(bdl)	0.60	(bdl)	0.03	0.32	95.6
10	E	high	(bdl)	32.1	(bdl)	(bdl)	0.15	64.8	(bdl)	0.87	0.06	0.02	0.40	98.9
11	E	intermediate	(bdl)	29.6	0.66	0.26	0.16	61.3	0.23	0.64	0.06	(bdl)	0.35	93.7
12	F	high	(bdl)	33.7	(bdl)	(bdl)	0.14	65.1	(bdl)	0.92	0.03	(bdl)	0.20	100.4
13	F	high	(bdl)	32.0	(bdl)	(bdl)	(bdl)	65.3	(bdl)	0.88	(bdl)	(bdl)	0.08	98.8
14	F	high	(bdl)	32.1	(bdl)	(bdl)	0.08	65.1	(bdl)	0.83	0.02	(bdl)	0.08	98.6
15	F	high	(bdl)	32.2	(bdl)	(bdl)	(bdl)	64.7	(bdl)	1.35	0.05	(bdl)	0.06	98.9
16	F	high	(bdl)	31.9	(bdl)	(bdl)	(bdl)	64.5	(bdl)	1.40	(bdl)	(bdl)	0.09	98.5
17	G	high	(bdl)	31.9	(bdl)	(bdl)	0.31	64.0	(bdl)	0.84	0.10	0.08	0.72	98.4
18	G	intermediate	(bdl)	31.4	0.92	0.26	0.30	62.8	(bdl)	1.65	0.19	0.09	0.85	99.2
19	H	high	(bdl)	31.9	(bdl)	(bdl)	0.23	64.0	(bdl)	0.85	0.15	0.09	0.87	98.3
20	H	low	(bdl)	30.8	1.81	0.13	0.29	62.2	0.14	0.58	0.04	0.11	1.01	98.1
21	H	low	(bdl)	30.8	1.50	0.10	0.29	62.6	0.15	0.52	0.10	0.09	0.89	97.6
22	I	high	(bdl)	32.0	(bdl)	0.09	0.29	64.0	(bdl)	1.00	0.11	0.07	0.86	99.0
23	I	low	(bdl)	30.5	2.09	0.27	0.21	61.6	(bdl)	0.43	0.04	0.07	0.86	96.3
24	J	high	(bdl)	31.8	(bdl)	0.09	0.38	63.4	0.23	1.32	0.21	0.16	1.17	99.3
25	J	low	(bdl)	30.6	1.21	0.04	0.38	61.9	0.14	0.82	0.24	0.13	1.14	96.8
26	K	high	(bdl)	31.7	(bdl)	0.09	0.10	64.3	(bdl)	0.48	0.02	0.02	0.22	97.7
27	K	high	(bdl)	31.7	(bdl)	(bdl)	(bdl)	64.6	(bdl)	0.64	(bdl)	(bdl)	0.22	97.5
Analyses in "macro-porous" interior regions:														
28	−	high	(bdl)	31.6	0.05	0.07	0.58	62.6	0.19	1.02	0.14	0.11	0.79	97.7
29	−	high	(bdl)	31.6	(bdl)	(bdl)	0.54	62.6	0.23	1.01	0.17	0.10	0.68	97.3
30	−	intermediate	(bdl)	30.3	0.89	0.33	0.49	61.2	0.16	0.94	0.14	0.08	0.73	95.5

Table 1, continued.

Analysis no.	Zone	BSE intensity	Al_2O_3	SiO_2	CaO	FeO	Y_2O_3	ZrO_2	Yb_2O_3	HfO_2	PbO	ThO_2	UO_2	Total
31	–	intermediate	(bdl)	30.5	0.78	0.22	0.69	61.0	0.18	1.04	0.23	0.11	0.93	96,2
32	–	low	(bdl)	30.0	3.17	0.58	0.57	58.2	0.20	1.01	0.03	0.10	0.92	95,3
33	–	low	(bdl)	30.4	1.64	0.43	(bdl)	61.9	(bdl)	1.30	0.04	(bdl)	0.40	96,8
34	–	low	0.16	29.7	2.18	0.61	0.62	59.3	(bdl)	0.93	0.03	(bdl)	0.38	94,4
35	–	low	(bdl)	30.3	3.55	0.75	0.58	57.7	(bdl)	1.05	(bdl)	0.08	0.80	95,7
36	–	low	(bdl)	30.3	2.68	0.48	0.48	59.8	0.18	1.09	0.06	0.10	0.81	96,4
37	–	low	(bdl)	30.2	3.14	0.40	0.22	59.5	(bdl)	1.05	(bdl)	(bdl)	0.42	95,3
38	–	low	(bdl)	30.1	2.48	0.41	(bdl)	60.4	(bdl)	0.42	(bdl)	0.02	0.55	95,3
39	–	high	(bdl)	31.5	(bdl)	(bdl)	0.47	62.6	0.17	1.19	0.12	0.09	0.79	97,5
40	–	high	(bdl)	31.5	(bdl)	(bdl)	0.60	62.6	0.16	0.89	0.13	0.10	0.83	97,4
41	–	intermediate	0.04	30.2	3.74	0.54	0.42	56.8	(bdl)	0.75	0.04	0.05	0.56	93,6
42	–	low	(bdl)	29.9	3.34	0.54	0.10	59.0	(bdl)	0.97	0.02	(bdl)	0.55	95,1
43	–	high	(bdl)	31.5	(bdl)	0.04	0.17	63.3	(bdl)	1.01	0.09	0.02	0.65	96,9
44	–	high	(bdl)	31.4	(bdl)	(bdl)	0.13	63.3	(bdl)	0.84	0.07	0.04	0.53	96,6
45	–	low	(bdl)	28.7	2.66	0.38	0.71	57.0	0.25	0.83	0.06	0.13	1.01	92,5
46	–	low	(bdl)	29.7	2.24	0.35	0.11	59.8	(bdl)	0.53	0.04	(bdl)	0.45	93,8
47	–	intermediate	(bdl)	30.2	1.23	0.27	(bdl)	60.9	0.14	0.90	0.05	0.02	0.51	94,7
48	–	low	(bdl)	30.6	3.81	0.54	0.66	57.4	0.13	1.24	0.02	0.14	1.06	96,5
49	–	intermediate	(bdl)	29.7	0.64	0.15	(bdl)	60.7	(bdl)	0.53	0.07	(bdl)	0.46	93,1
50	–	high	(bdl)	31.3	0.06	(bdl)	0.69	61.8	0.12	1.02	0.16	0.15	0.90	96,7
51	–	high	(bdl)	31.8	(bdl)	(bdl)	0.08	64.2	(bdl)	1.47	0.02	(bdl)	0.20	98,5
52	–	low	(bdl)	30.5	3.48	0.81	0.66	57.1	0.23	0.94	0.04	0.14	1.14	95,6
53	–	intermediate	(bdl)	30.3	1.28	0.28	0.24	60.8	0.14	1.19	0.12	0.02	0.68	95,7
54	–	low	(bdl)	29.9	3.59	0.72	0.10	58.6	0.15	0.94	(bdl)	(bdl)	0.58	95,2
Detection limit**	0.04	0.1	0.04	0.07	0.07	0.1	0.12	0.20	0.02	0.02	0.02	–		

Table 2. Results of SHRIMP U−Pb isotopic analyses.

Analysis no.	BSE intensity	U (ppm)	Th (ppm)	Th/U	Pb (ppm)	f 206* (%)	$^{206}Pb/^{238}U$	$^{206}Pb/^{238}U$ age (Ma)	$^{207}Pb/^{206}Pb$	$^{207}Pb/^{206}Pb$ age (Ma)	Disc.** (%)
Analyses in "zoned" interior regions:											
1	low	6339	681	0.11	933	0.01	0.1549 ± 0.0031	928 ± 17	0.07372 ± 0.00012	1031 ± 3	11
2	high	7585	843	0.11	1421	0.00	0.1970 ± 0.0039	1159 ± 21	0.07424 ± 0.00009	1045 ± 3	-12
3	low	5249	627	0.12	886	0.01	0.1761 ± 0.0035	1046 ± 19	0.07459 ± 0.00012	1055 ± 3	1
4	high	6344	749	0.12	933	0.01	0.1825 ± 0.0031	1081 ± 20	0.07456 ± 0.00011	1054 ± 3	-3
5	high	1254	40	0.03	204	0.00	0.1742 ± 0.0034	1035 ± 19	0.07460 ± 0.00028	1055 ± 8	2
6	low	8036	915	0.11	1475	0.00	0.1927 ± 0.0041	1136 ± 22	0.07412 ± 0.00019	1042 ± 5	-10
7	low	4967	478	0.10	301	0.05	0.0644 ± 0.0013	402 ± 8	0.06149 ± 0.00038	654 ± 13	40
8	high	604	30	0.05	95	0.05	0.1671 ± 0.0033	996 ± 18	0.07468 ± 0.00044	1057 ± 12	6
9	low	4260	365	0.09	681	0.01	0.1691 ± 0.0033	1007 ± 18	0.07459 ± 0.00014	1055 ± 4	5
10	low	5835	594	0.10	802	0.02	0.1447 ± 0.0029	871 ± 16	0.07410 ± 0.00007	1041 ± 2	17
11	high	1696	295	0.17	292	0.03	0.1777 ± 0.0035	1054 ± 19	0.07486 ± 0.00022	1062 ± 6	1
12	high	982	129	0.13	170	0.05	0.1807 ± 0.0036	1071 ± 20	0.07461 ± 0.00028	1055 ± 8	-2
13	low	3794	283	0.07	663	0.00	0.1854 ± 0.0037	1096 ± 20	0.07468 ± 0.00013	1057 ± 3	-4
14	low	3244	249	0.08	370	0.11	0.1083 ± 0.0021	663 ± 12	0.07082 ± 0.00024	949 ± 7	32
15	high	6836	817	0.12	1173	0.01	0.1800 ± 0.0036	1067 ± 19	0.07411 ± 0.00010	1042 ± 3	-3
16	high	4131	309	0.07	730	0.01	0.1876 ± 0.0037	1108 ± 20	0.07422 ± 0.00013	1045 ± 3	-7
Analyses in "macro-porous" interior regions:											
17	low	8979	1391	0.15	608	0.04	0.0708 ± 0.0015	441 ± 9	0.06262 ± 0.00039	693 ± 13	38
18	low	8324	989	0.12	643	0.02	0.0815 ± 0.0018	505 ± 11	0.06395 ± 0.00050	737 ± 16	33
19	low	4109	463	0.11	595	0.01	0.1521 ± 0.0030	913 ± 17	0.07410 ± 0.00015	1041 ± 4	13
20	low	4727	53	0.01	693	0.03	0.1574 ± 0.0033	942 ± 18	0.07411 ± 0.00030	1042 ± 8	10
21	low	4416	301	0.07	347	0.00	0.0837 ± 0.0019	518 ± 11	0.06485 ± 0.00052	767 ± 17	34
22	low	4953	489	0.10	579	0.01	0.1226 ± 0.0024	745 ± 14	0.07122 ± 0.00071	961 ± 20	24
23	low / intermediate	8461	1425	0.17	1417	0.00	0.1737 ± 0.0034	1033 ± 19	0.07373 ± 0.00009	1031 ± 2	0
24	low	1973	12	0.01	170	0.11	0.0917 ± 0.0021	565 ± 12	0.06977 ± 0.00031	919 ± 9	40
25	low	5895	848	0.14	852	0.00	0.1508 ± 0.0030	905 ± 17	0.07348 ± 0.00012	1025 ± 3	12
26	low	4310	1169	0.27	619	0.02	0.1486 ± 0.0030	893 ± 17	0.07266 ± 0.00013	1002 ± 4	12